



Research Article

Enhancement of antibacterial and anticancer properties of pure and REM doped ZnO nanoparticles synthesized using *Gymnema sylvestre* leaves extract

M. Karthikeyan¹ · A. Jafar Ahamed¹ · C. Karthikeyan² · P. Vijaya Kumar³

© Springer Nature Switzerland AG 2019

Abstract

Zinc oxide (ZnO) (K1) doped with rare earth metals (REM) such as lanthanum doped ZnO (K2), cerium doped ZnO (K3) and neodymium doped ZnO (K4) nanoparticles (NPs) were synthesized by green method using *Gymnema sylvestre* (*G. sylvestre*) leaves extract as reducing as well as capping agent and this method was also one of the alternatives to conventional physical and chemical methods. The synthesized K1, K2, K3 and K4 samples were characterized by X-ray diffraction analysis (XRD), X-ray photoelectron spectroscopy (XPS), field emission scanning electron microscopy (FESEM), energy dispersive X-ray spectroscopy (EDAX), Fourier transform infrared spectroscopy (FTIR), UV–visible spectroscopy, photoluminescence (PL) techniques and electron para magnetic resonance (EPR) spectroscopy. The K1, K2, K3 and K4 samples were tested against clinical pathogens such as gram positive G+ (*Staphylococcus aureus* and *Streptococcus pneumoniae*) and gram negative G– (*Klebsiella pneumoniae*, *Shigella dysenteriae*, *Escherichia coli*, *Pseudomonas aeruginosa* and *Proteus vulgaris*) bacterial strains using well diffusion method. The K2 sample shows higher antibacterial effect when compared to K1, K3 and K4 samples. In vitro cytotoxicity effect was analysed for A498 (human kidney carcinoma) cell line and normal vero (African monkey kidney) cell lines.

Keywords ZnO nanoparticles · *Gymnema sylvestre* · Rare earth metals · XPS · EPR · Antibacterial and anticancer

1 Introduction

Recently, rare earth metal (REM) ions doped semiconductor NPs are used in various fields such as optical, electronic and magnetic devices [1–6]. Since, ZnO NPs exhibit unique characteristics like low cost, nontoxicity, eco-friendly system to the nature and easy to prepare compounds with various morphologies having different properties. However, ZnO NPs is an n-type semiconductor with wide direct band gap (3.37 eV) and large excitation binding energy (60 meV) at room temperature.

Nano sized ZnO can be potentially important with numerous applications such as solar cells [7], gas sensors [8], photocatalytic, antibacterial, electrical and optical

devices [9], electrostatic dissipative coatings [10], degradation of environmental pollutants [11, 12] and external uses as antibacterial agents in lotions, mouthwashes, ointments and surface coatings to prevent microbial growth [13]. The REM-doped ZnO NPs are vibrant materials for flat panel displays for efficient emission in the visible range. On other hand, ZnO NPs is one of the environmental friendly materials. The REM-doped ZnO NPs may be used as fluorescence labels for biological medical imaging [14].

Chemically synthesized nanoparticles by-products are toxic to the environment [15]. Among this, to avoid the toxic by-products green synthesis using the bio-materials such as microorganisms and plants or plant extracts

✉ A. Jafar Ahamed, agjafar@yahoo.co.in | ¹Department of Chemistry, Jamal Mohamed College (Autonomous), Tiruchirappalli, Tamil Nadu 620 020, India. ²KIRND Institute of Research and Development Pvt Ltd., Tiruchirappalli, Tamil Nadu 620 020, India. ³Department of Chemistry, Asan College of Arts and Science, Karur, Tamil Nadu 639 003, India.



derived metal oxide nanoparticles can be an effective alternative method for chemical synthesis. Various biological sources are used for green synthesis like plant [16], bacteria [17], fungi [18] and yeast [19].

Among them *G. sylvestre* belongs to *Asclepiadaceae* family group, which is potentially used for treatment of asthma, eye complaints and snake bites [20]. This leaves extract holds a large number of bioactive compounds such as benzene-1,2-diol, 3-Allyl-2-methoxyphenol, hexadecanoic acid, octa decanoic acid [21], saponins (*Gymnemic acid*) and tannins [22]. Vijaya Kumar et al. have reported that *Gymnemic acid* has been a good reducing agent to prepare the metal oxide nanoparticles [23].

The metal oxide nanomaterials have been potentially used in biomedical applications, which may be due to the high surface area of metal oxide NPs. It has considerably enhanced its ability to produce reactive oxygen species (ROS) [24, 25]. ROS production may be effected by various paths such as irradiance of nanomaterials by ultraviolet (UV) light, disturbance of intracellular metabolic activities, and antioxidant system. This results in the generation of oxidative stress in the cells. ROS can cause cell death in the DNA, cell membrane, and proteins [26, 27].

In the present investigation, pure and REM ions (La^{3+} , Ce^{3+} , and Nd^{3+}) doped ZnO NPs were synthesized by green method using *G. sylvestre* leaves extract. The

structural, optical, antibacterial and anticancer properties of the pure and REM-doped ZnO NPs have been studied in this work.

2 Experimental methods

2.1 Synthesis of pure and REM doped ZnO NPs by using *G. sylvestre* leaves extracts

Gymnema sylvestre leaves was taken and washed several time with tap and double distilled water. After that 15 g of leaves was taken in 150 ml of deionized water in a beaker and boiled at 80 °C for 1 h. The prepared leaves extract was filtered using Whatman-1 filter paper.

In the case of ZnO NPs, 0.1 M $\text{Zn}(\text{NO}_3)_2 \cdot 6\text{H}_2\text{O}$ solution was dissolved into 150 ml of *G. sylvestre* leaves extract. Homogenously mixed nitrate solution was continuously stirred at 80 °C for 6 h. An yellow colour precipitate was obtained. Further the precipitate was dried at 120 °C for 2 h. The obtained ZnO nanopowder were annealed at 700 °C for 5 h and stored in an airtight container.

Similarly, for La-doped ZnO sample, 0.002 M $\text{La}(\text{NO}_3)_3 \cdot 6\text{H}_2\text{O}$ was added into 0.098 M $\text{Zn}(\text{NO}_3)_2 \cdot 6\text{H}_2\text{O}$ and dissolved in 150 ml of *G. sylvestre* leaves extract and the above homogeneously mixed solution was stirred constantly at 80 °C for 6 h. The yellow colour precipitate obtained, was dried at 120 °C for 2 h, to get La doped ZnO

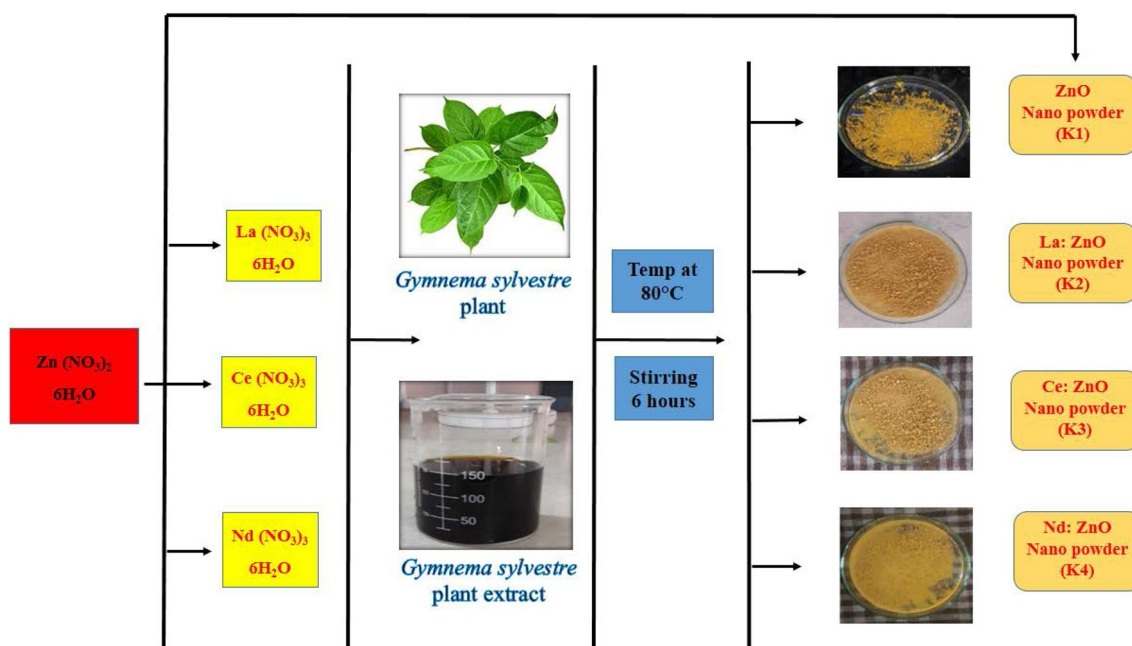


Fig. 1 Schematic diagram for the formation of K1, K2, K3 and K4 samples

nanopowder. The obtained nanopowder was annealed at 700 °C for 5 h. The above procedure was followed for the preparation of the Ce, and Nd doped ZnO samples. Thus, ZnO (K1), La doped ZnO (K2), Ce doped ZnO (K3) and Nd doped ZnO (K4) samples were obtained. Figure 1 shows the schematic diagram of synthesized K1, K2, K3 and K4 samples.

absorbance for each well was measured at 570 nm using a micro plate reader (Thermo Fisher Scientific, USA) and the percent K1, K2, K3 and K4 samples cell viability and IC₅₀ value was calculated using GraphPad Prism 6.0 software (USA). The data were collected for three replicates. The percentage of inhibition was calculated from this data using the formula

$$\% \text{ of inhibition} = \frac{\text{mean OD of untreated cells (control)} - \text{mean OD of treated cells}}{\text{mean OD of untreated cells (control)}} \times 100.$$

2.2 Antibacterial assay

The antibacterial activity of the K1, K2, K3 and K4 samples was studied against gram positive G+ (*Staphylococcus aureus* and *Streptococcus pneumoniae*) and gram negative G- (*Klebsiella pneumoniae*, *Shigella dysenteriae*, *Escherichia coli*, *Pseudomonas aeruginosa* and *Proteus vulgaris*) bacterial strains using well diffusion method. Petri plates were prepared with 25 ml of sterile Muller Hinton agar (MHA, Himedia) and each bacterial pathogen was individually swabbed on MHA in separate plates. The antibacterial activity was tested at a concentration of 1.5 mg/ml with the required quantity of the NPs dispersed in dimethyl sulphoxide (DMSO). The zone of inhibition levels (mm) were measured after 24 h and before this step, it was incubated overnight at 37 °C. The standard antibiotic Amoxicillin was used as the positive control.

2.3 Cell culture

A498 (kidney carcinoma cell) and Vero (African monkey kidney cell) cell line were cultured in liquid medium DMEM (Dulbecco's modified eagle's medium) supplemented 10% Fetal Bovine Serum (FBS), 100 µg/ml penicillin and 100 µg/ml streptomycin, and maintained under an atmosphere of 5% CO₂ at 37 °C.

2.4 MTT assay

The K1, K2, K3 and K4 samples were tested for in vitro cytotoxicity, using A498 and Vero cells by 3-(4,5-dimethylthiazol-2-yl)-2,5-diphenyltetrazolium bromide (MTT) assay [28]. The synthesized K1, K2, K3 and K4 samples were suspended with sterile phosphate buffer (PBS) and treated with various concentrations 10–100 µg/ml in a serum free DMEM medium to treat the chosen cell line A498 and Vero cell. Each sample was replicated three times and the cells were incubated at 37 °C at 24 h and each well, 20 µl of 5 mg/ml MTT in phosphate buffer (PBS) was added. The

2.5 Characterization studies

The K1, K2, K3 and K4 samples were analysed by X-ray diffractometer (model: X'PERT PRO PANalytical). The morphological features of the sample were measured by Field emission scanning electron microscopy (Model: Carl Zeiss 55) with EDAX (Ultra 55). The FT-IR spectrum was recorded in the range of 400–4000 cm⁻¹ by using Perkin-Elmer spectrometer. Ultraviolet–visible spectra of the sample was measured on a Perkin-Elmer UV-Lambda 25 spectrophotometer (Perkin-Elmer, Norwalk, Connecticut). The PL emission study of the sample was carried out using Horiba Jobin–YVON spectrofluorometer (model: FLUORO-MAX-4, 450 W high pressure Xenon lamp as the excitation source, photomultiplier at a range 325–550 nm). The XPS measurements were performed with an XPS instrument (Carl Zeiss) under-high vacuum with Al K_α excitation at 250 W. To obtain information on defects and vacancies, EPR was recorded using X-band JEOL JES-RE1X at the room temperature.

3 Results and discussion

3.1 X-ray diffraction studies

Figure 2 shows the XRD patterns of the K1, K2, K3 and K4 samples using *G. sylvestre* leaves extract. The XRD peaks position are located at (100), (002), (101), (102), (110), (103), (112), (201), (004) and (202) for ZnO NPs, retained hexagonal wurtzite structure of ZnO NPs with the p63mc space group corresponding to JCPDS data (Card No. 36-1451). In the case of REM doped ZnO NPs, there is no impurity phase observed in La³⁺ and Nd³⁺ samples. Furthermore, the ZnO doped with Ce NPs have one additional peak observed corresponding to 2θ = 28.573 (JCPDS No 34-0394). This is due to the partial oxidation of Ce³⁺ into Ce⁴⁺, through the formation of CeO₂. The XRD parameters like lattice constant, atomic peaks factor c/a, Cos(φ), position parameter (u) and bond length (L) estimated through the literature

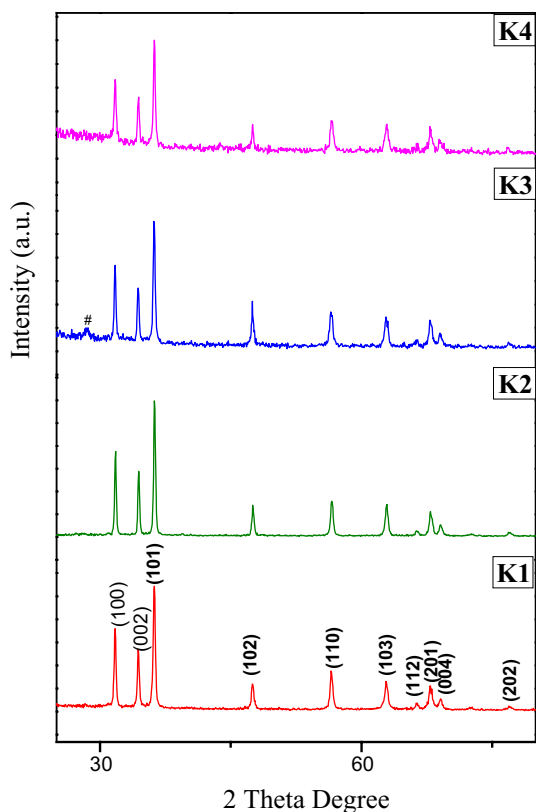


Fig. 2 X-ray powder diffraction patterns of K1, K2, K3 and K4 samples

[29] and the values are given in the Table 1. The small shift is observed for the REM doped ZnO NPs compared to the pure ZnO NPs.

The crystallite size (*D*) of pure ZnO NPs is determined by the X-ray line broadening method using the Scherrer's equation,

$$D = \frac{k\lambda}{\beta_{D\cos\theta}} \tag{1}$$

where *D* is the size in nanometers, λ is the wavelength of radiation (1.5406 Å for CuK α), *k* is a constant (0.94), β_D is the peak width at half-maximum intensity and θ is the peak position.

The average crystalline size observed at 38, 33, 27 and 23 nm correspond to K1, K2, K3 and K4 samples respectively. The REM doped ZnO NPs possess decreased size than the pure ZnO NPs, which may be due to alteration in the host ZnO matrix through the foreign impurities i.e., La³⁺, Ce³⁺, and Nd³⁺.

3.2 Morphology and elemental composition studies

Figure 3a–d shows the FESEM images for K1, K2, K3 and K4 samples. From the FESEM images, the K1, K2, K3 and K4 samples form a spherical, spindle, hexagonal and flake like nanostructures. The average particles size were observed at 138 nm, 52 nm, 59 nm, and 63 nm for K1, K2, K3 and K4 samples respectively. The average thicknesses was reduced for REM ions doped ZnO as compared to the pure ZnO NPs respectively. The reduction in thickness is attributed to the distortion in the ZnO matrix incorporated with rare earth metal ions like La³⁺, Ce³⁺, and Nd³⁺. These doping materials are of different ionic radii such as La³⁺(1.061 Å), Ce³⁺(1.034 Å) and Nd³⁺(0.995 Å) and hence, the substitution of the REM with ZnO matrix obviously changes the morphology of the REM doped ZnO nanoparticles namely K1, K2, K3 and K4 samples [29].

The chemical composition of K1, K2, K3 and K4 samples are shown in Fig. 3e–h. In the case of doping samples K2, K3 and K4, the atomic percentage of La, Ce, and Nd are estimated as 11.90%, 7.18%, and 9.98% respectively. For K1 sample atomic percentage of Zn and O are observed at 83.90% and 16.10% respectively. For REM ions (La³⁺, Ce³⁺, and Nd³⁺)-doped ZnO NPs, zinc percentage increases whereas oxygen percentage decreases as compare to the pure ZnO NPs. The chemical composition values are given in the Table 2.

Table 1 X-ray diffraction parameter values of the K1, K2, K3 and K4 samples

Samples	Lattice parameter values (nm)		Atomic packing factor (c/a)	Volume (V) (Å) ³	Cos ϕ	Position parameter (u)	Bond length (Zn–O) L (Å)	Average crystallite size <i>D</i> (nm)
	a	c						
K1	0.3255	0.5215	1.6017	47.876	0.9459	0.3798	1.5569	38
K2	0.3251	0.5209	1.6025	47.689	0.9578	0.3798	1.5555	33
K3	0.3258	0.5217	1.6011	47.988	0.9465	0.3800	1.5579	27
K4	0.3251	0.5214	1.6039	47.733	0.9464	0.3799	1.5551	23

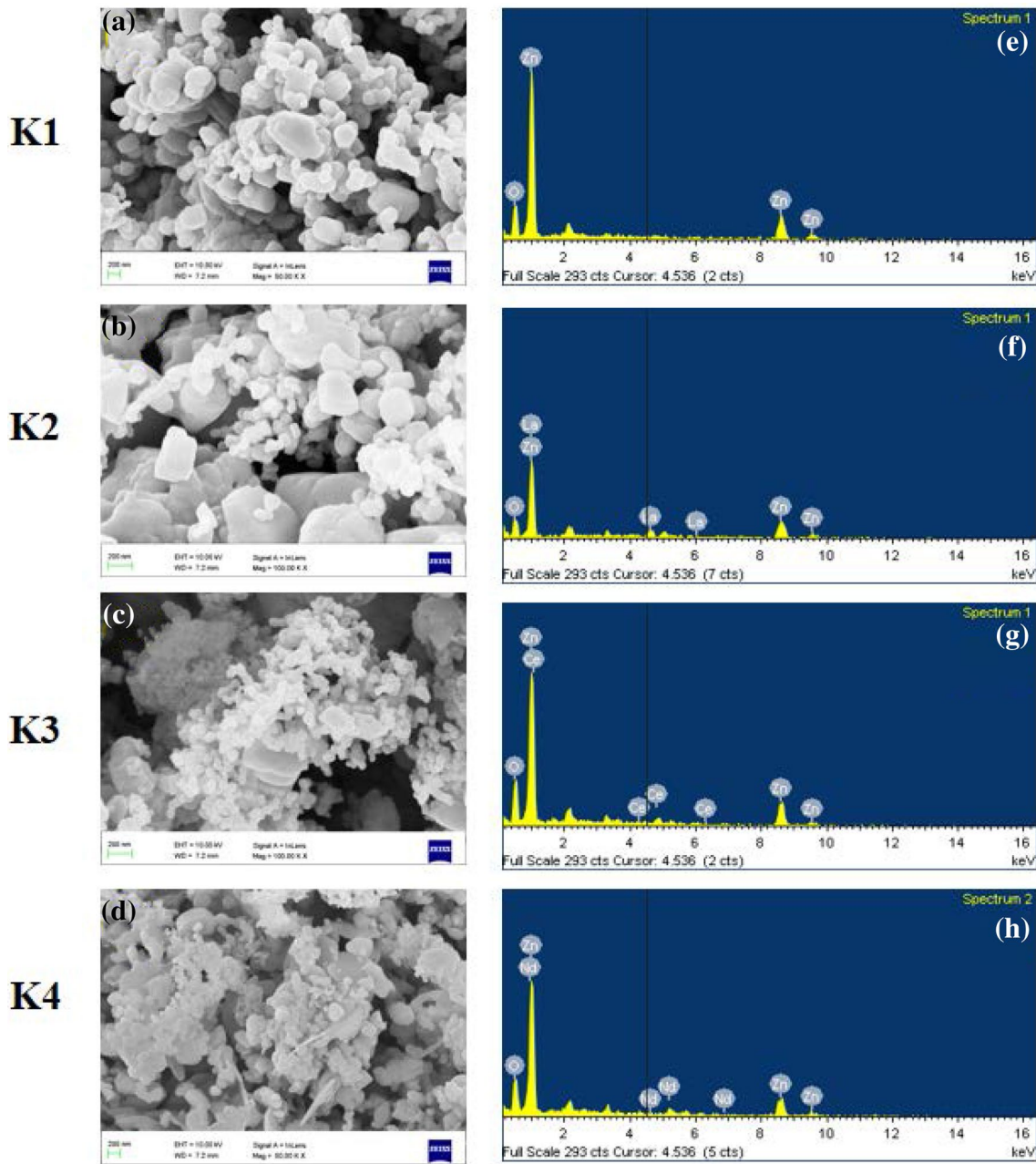


Fig. 3 Morphology of a–d K1, K2, K3 and K4 samples and elemental composition of e–h K1, K2, K3 and K4 samples

Table 2 The elemental composition of the synthesized K1, K2, K3 and K4 samples

Samples	at%			
	Zn	O	Doping amount	Total (%)
K1	83.90	16.10	–	100
K2	76.92	11.17	11.90 (La)	100
K3	76.29	16.52	7.18 (Ce)	100
K4	71.05	18.97	9.98 (Nd)	100

3.3 Fourier transform infra-red (FT-IR) spectroscopic studies

Figure 4 shows FT-IR spectra of K1, K2, K3 and K4 samples. In the present investigation, wide O–H stretching band has been observed at 3420 cm^{-1} for K1 sample, which may be surface absorbed water molecule [30]. The asymmetric C–H stretching band is located at 2978 cm^{-1} for K1 sample. The narrow intense H–O–H bending centred

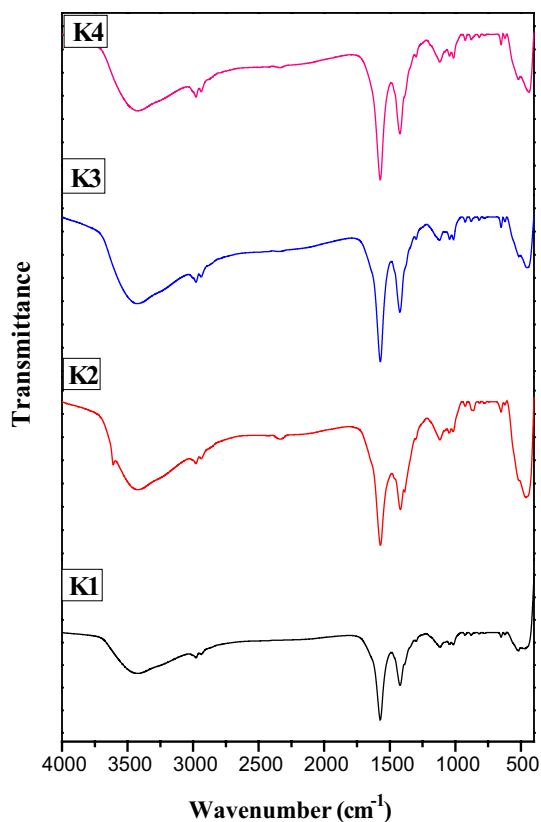


Fig. 4 FTIR spectrum of K1, K2, K3 and K4 samples

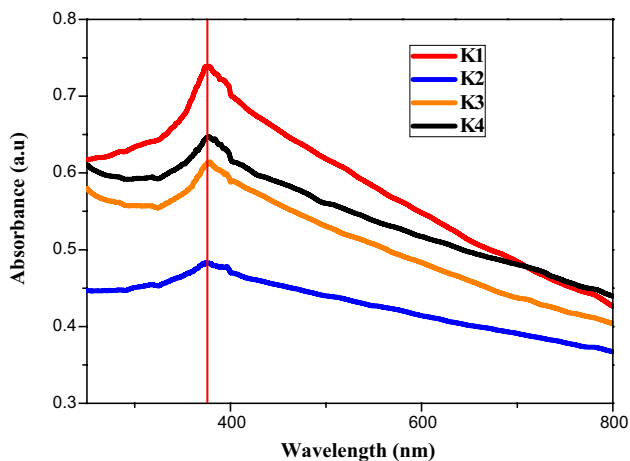


Fig. 5 Absorption spectra of K1, K2, K3 and K4 samples

at 1571 cm^{-1} . The medium intensity band 1424 cm^{-1} is attributed to C=O symmetric stretching. The O–H asymmetric stretching bands found to be 1044 and 1014 cm^{-1} for K1 sample. The weak Metal–Oxygen (Zn–O) vibration frequencies are observed at 878 and 817 cm^{-1} for

K1 sample. The medium intense peak at 467 cm^{-1} was recognized as the Zn–O stretching band. The REM doped ZnO NPs vibration frequencies small shift occur as compared to pure ZnO NPs. The metal–oxygen (Zn–O) vibration frequency ($467\text{--}461\text{ cm}^{-1}$) ($467\text{--}452\text{ cm}^{-1}$) and ($467\text{--}439\text{ cm}^{-1}$) for K2, K3, and K4 samples respectively, due to the REM La^{3+} , Ce^{3+} and Nd^{3+} ions substitution in the ZnO matrix.

3.4 UV–Vis spectroscopic studies

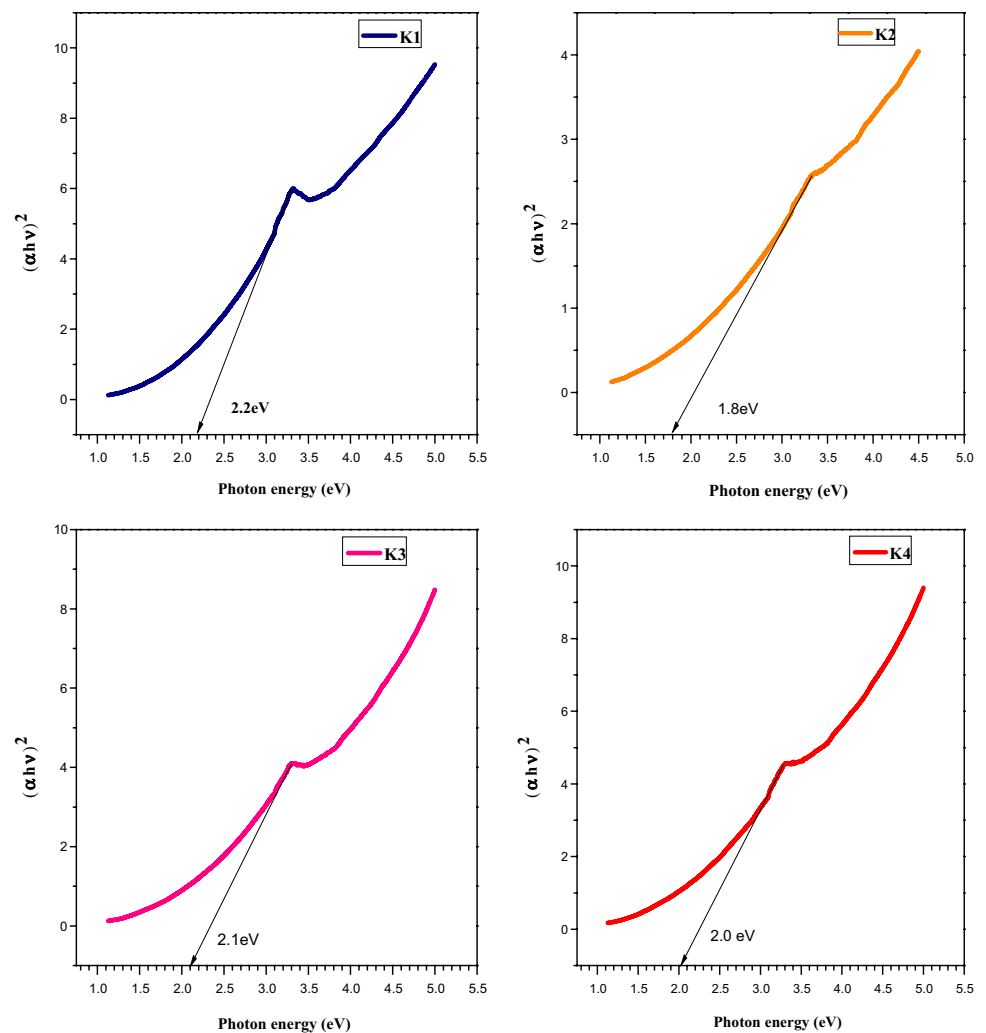
UV–Visible spectra of K1, K2, K3 and K4 samples are shown in Fig. 5. 3 mg of pure and doped samples were uniformly dispersed in distilled water and the solution was ultra sonificated for 20 min before recording UV–Vis absorbance spectra. The K1, K2, K3 and K4 samples exhibited strong absorption edge peaks at 378, 377, 376, and 374 nm respectively. The REM doped ZnO NPs are blue shifted when compared to pure ZnO NPs, which may be due to the doping induced effects. The band gap energy are calculated using Tauc relation [31]. A plot (Fig. 6) between $(\alpha h\nu)^2$ and photon energy (eV) is drawn for K1, K2, K3 and K4 samples. The optical band gap of K1, K2, K3 and K4 samples are observed at 2.2, 1.8, 2.1 and 2.0 eV respectively. The K1, K2, K3 and K4 samples band gap results are compared with commercially available TiO_2 (for 3.1 eV) and ZnO (for 3.37 eV) [32]. The green synthesized K2 sample band gap energy (for 1.8 eV) is lower than the commercially available TiO_2 and ZnO NPs. This result showed that K2 sample can be more effectively used as photocatalyst.

3.5 Photoluminescence (PL) studies

Figure 7 shows the photoluminescence spectra of K1, K2, K3 and K4 samples using an excitation wavelength of 325 nm. In the case of K1 sample, the emission wavelengths are observed at 421, 451, 465, 489 and 516 nm respectively. The violet emission centered at 421 nm is ascribed to an electron transition from a shallow donor level of the natural zinc interstitials to the top level of the valence band [33]. The two blue emissions located at 451 and 465 nm are due to the singly ionized Zn vacancies [34]. The blue green emission observed at 489 nm is ascribed to the transition between the oxygen vacancy and interstitial oxygen [35]. Finally green emission observed at 516 nm, corresponds to the singly ionized oxygen [36, 37].

The PL emission band values for K1, K2, K3 and K4 NPs are given in Table 3. Green emission band disappear for K4 sample as compared to K1 sample, due to the distortion

Fig. 6 Tauc plots of $(\alpha h\nu)^2$ versus photon energy used to estimate optical band gap of K1, K2, K3 and K4 samples



in the host ZnO lattice by the REM ion impurities. However for the K2 sample, green emission values (522 nm) increased as compared to the K1 (516 nm) and K3 (510 nm) samples respectively. These changes in emissions, confirm that REM (La^{3+} , Ce^{3+} and Nd^{3+}) ions incorporate with ZnO matrix.

3.6 XPS studies

XPS spectra of K1, K2, K3 and K4 samples are shown in Fig. 8. The Zn (2p), O (1s), La (3d), Ce (3d) and Nd (3d) oxidation states were identified using XPS spectra. The Zn (2p) singlet split in two doublets, such as Zn $2p_{1/2}$ and Zn $2p_{3/2}$ observed at 1045.327 and 1022.214 eV respectively, which is attributed to the ZnO matrix for the K1 sample had Zn^{2+} being bound to oxygen [29]. The K3 and K4 samples binding energy values are increased. In the case of K2 sample binding energy values are decreased,

due to the ions residing partially in the tetrahedral Zn positions [29].

Figure 9 shows the O (1s) spectra of K1, K2, K3 and K4 samples. The green synthesized K1 sample of O (1s) signal observed at 531.115, 532.710 and 533.821 eV respectively. The lower binding energy O (1s) signal centre at 531.115 eV, which may be O_2^- ion in the wurtzite. The middle and higher binding energy located at 532.710 and 533.821 eV are attributed to the loosely-bound oxygen, like absorbed O_2 or adsorbed H_2O on the ZnO surface. The REM doped ZnO NPs binding energy of O (1s) values are observed as positional shift which is not observed in the case of K1 sample. This alteration may be charge due to the transfer efficiency from Zn^{2+} to O_2^- ions. These results strongly affected surface defects and vacancies, leading to increasing the charge-transferring efficiency in the metal ions.

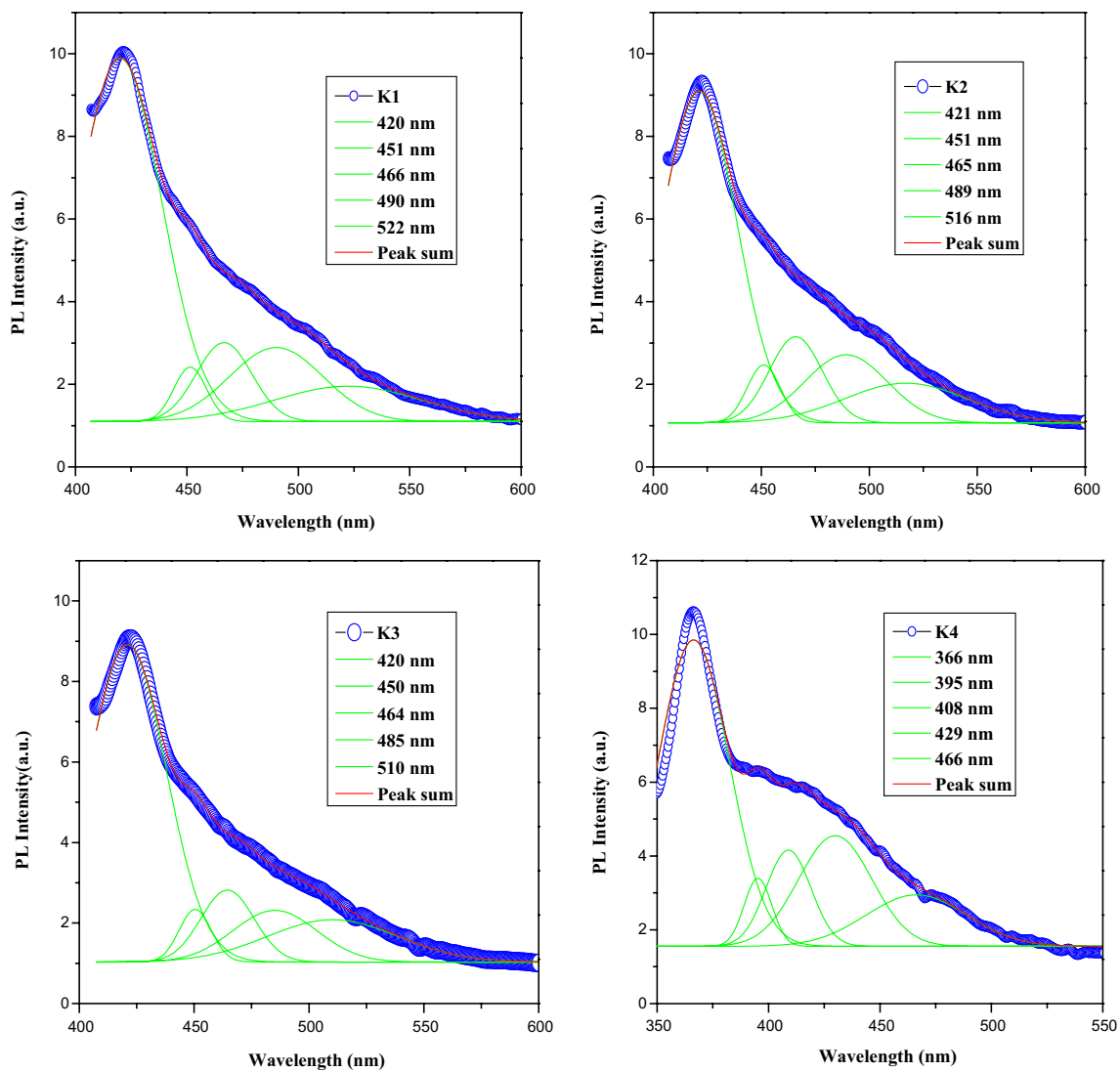


Fig. 7 PL emissions spectra of K1, K2, K3 and K4 samples using the excitation wavelength at 325 nm

Table 3 Gaussian decomposed photoluminescence emission values of K1, K2, K3 and K4 samples

K1 (nm)	K2 (nm)	K3 (nm)	K4 (nm)
421	420	420	366
451	451	450	395
465	466	464	408
489	490	485	429
516	522	510	466

The 3d spectra for K2, K3 and K4 samples are shown in Fig. 10a–c. The La (3d) signal split into La 3d_{5/2} and La 3d_{3/2} observed at (836.42 and 839.92 eV) and (853.34 and 856.35 eV) for K2 sample respectively [38]. The Ce (3d) signal is divided into Ce 3d_{3/2} and Ce 3d_{5/2} state

located at 906.40 and 879.34 eV for K3 sample respectively. The signals for Nd (3d) are found at 976.28, 982.35, 992.11 and 1003.01 eV for K4 sample. It can be seen that La³⁺, Ce³⁺ and Nd³⁺ ion substitution in ZnO matrix, not only changes the atomic arrangement but also gradually tunes their electronic structures.

3.7 Antibacterial activity

The antibacterial activities of green synthesized ZnO (K1), La doped ZnO (K2), Ce doped ZnO (K3) and Nd doped ZnO (K4) NPs are treated with concentration 1.5 mg/ml and it is shown in Fig. 11. Day by day, more number of researchers are focused to study antibacterial activity of ZnO and doped ZnO NPs. But their doped concentration and their antibacterial results are varied. So, currently we

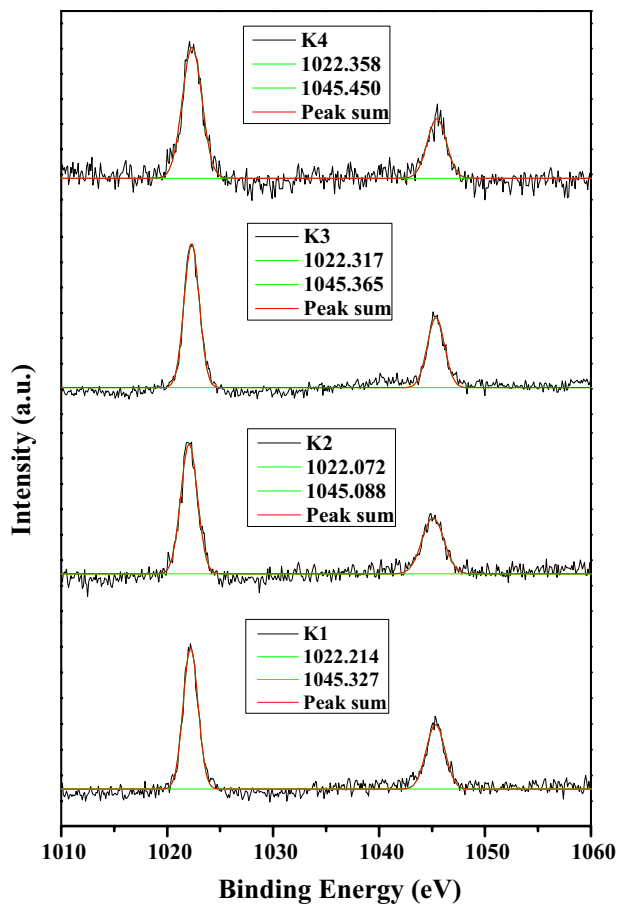


Fig. 8 XPS spectra of Zn (2p) for K1, K2, K3 and K4 samples

focused on the enhanced antibacterial activity of ZnO NPs. From this study, the K2 sample shows more antibacterial effect than K1, K3 and K4 samples. Table 4 shows a comparison between present and reported concentration values of various metals doped ZnO NPs required to inhibit the growth of human pathogens [31, 39–43]. The zone of inhibition (ZOI) of human pathogens is shown in Fig. 12. The photo-generation of ZnO NP's reactive oxygen species (ROS) are accountable for various factors such as surface area, oxygen vacancies, and Zn^{2+} ions release [43]. The K1, K2, K3 and K4 NPs exhibits antibacterial activity as shown in Fig. 12. However, the K2 sample shows the highest antibacterial activity. In early report, the appropriate crystallite size (ca. 33 nm) caused higher antibacterial effects [29, 44]. From XRD results the particles size of the NPs are found to be 38, 33, 27 and 23 nm for K1, K2, K3 and K4 samples respectively. The K2 sample exhibits 33 nm for crystallite size, is ascribed to higher antibacterial activity. From the antibacterial activity, the NPs with uneven surfaces and rough edges have been found to adhere to the

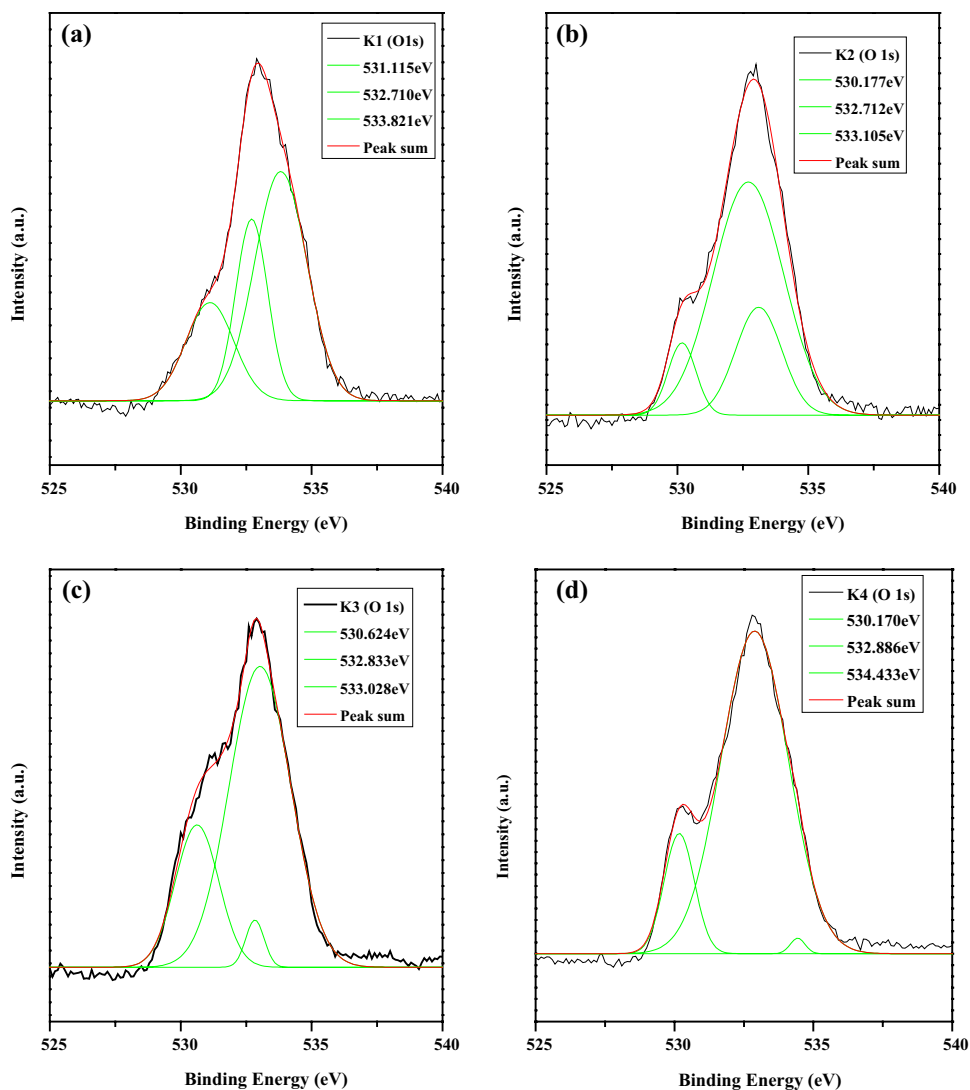
bacterial wall and cause damage to the cell membrane [29]. From the FESEM image, it clear shows different morphologies like spherical, spindle, hexagonal and flake structures for K1, K2, K3 and K4 samples respectively. La-doped ZnO NPs [K2] have uneven ridges at their outer surface which led to antibacterial activity, whereas the other NPs have smooth surfaces, which indicates that antibacterial activity is effective in uneven ridged surfaces. The EPR spectra provides information about the native defects in K1, K2, K3 and K4 samples as shown in Fig. 13. In early literatures, [28, 45, 46] the ZnO NPs (K1) higher intensity of the signal are associated with more oxygen vacancies (V_o) in it. Therefore, according to Fig. 13, the higher intensity are observed for K1, K3 and K4 samples as compared to K2 samples. This result shows that the amount of oxygen vacancies in the K2 sample is more than that in the K1 sample. From antibacterial test, we conclude that K2 sample render an effective antibacterial agent as compared to the K1, K3 and K4 samples. Based on the comparative statement, the present study confirmed that the pure and doped ZnO NPs exhibit moderate antibacterial activities respectively. It is worth to mention that all the samples exhibit strong antibacterial activity towards both G+ and G- bacterial culture.

3.8 In vitro toxicity studies on normal vero cell versus kidney cancer cell line

The ZnO NPs is a wide band-gap semiconductor and photo excitation under the UV lights, whose energy has greater than the band gap energy [47]. The photo excitation of ZnO initiates electron transfer from the valence band to the conduction band, its creating an electron-hole pair. In general, the holes in the valence band act as oxidants and thus generate hydroxyl radicals ($\cdot OH$) upon reaction with water. The electrons in the conduction band reduce oxygen to produce superoxide anions (O_2^-) [47]. Reactive oxygen species (ROS) generation by ZnO NPs upon irradiation with UV light has been utilized for photo-triggered anticancer activities via ROS-induced damage the cell membranes, mitochondria, proteins, and DNA [48–51].

The cytotoxicity of the K1, K2, K3 and K4 samples were tested at various concentration 10–100 $\mu g/ml$ for A498 (Kidney carcinoma cell) and Vero (African green monkey kidney cell) cell lines. The IC_{50} value of (41.74, 35.86, 40.05 and 63.08 $\mu g/ml$) and (55.27, 49.69, 56.83 and 51.10 $\mu g/ml$) (evaluated after 24 h) of K1, K2, K3 and K4 samples against A498 and Vero cells was ($p \leq 0.05$ $p < 0.01$). The La-doped ZnO (K2) sample showed a highly effective cytotoxic activity against A498 and Vero cells

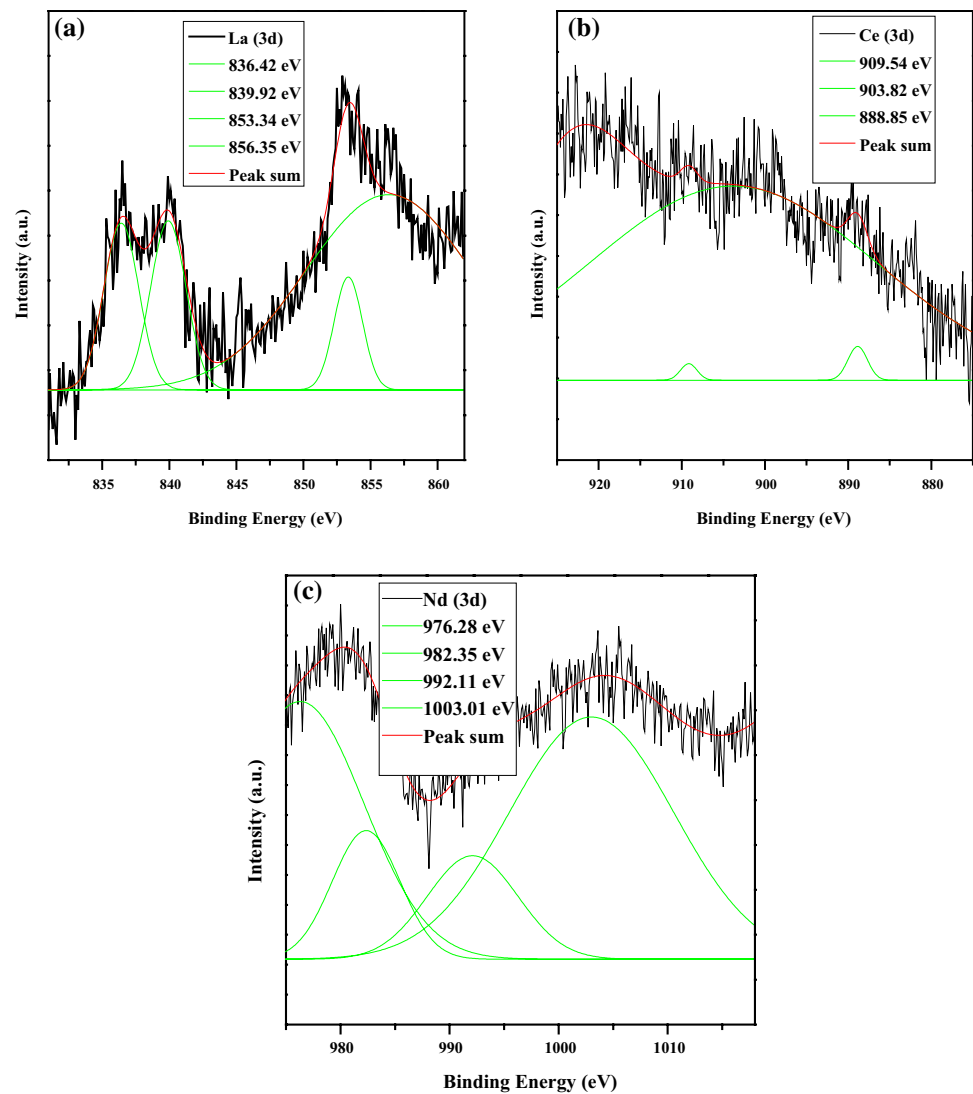
Fig. 9 XPS spectra of O (1s) for K1, K2, K3 and K4 samples



(Fig. 14a, b). Table 5 shows a comparison between our and earlier reported IC_{50} values of ZnO NPs [42, 52–58]. Cell morphological changes were observed for light microscope with different concentrations 10, 50 and 100 $\mu\text{g/ml}$ (Fig. 15).

As per the early discussion, the cytotoxicity effect of ZnO NPs potentially depends on the attendance of higher ROS, ZnO induced a reduced band gap due to

the increased redox capability. The enhancement in the anticancer activity in La doped ZnO NPs is due to the increased production of the reactive oxygen species (ROS) in the presence of La^{3+} ions and ZnO in the presence of UV light [59]. However, La doped ZnO (K2) sample, show enhanced ability to produce photo generated holes (h^+), resulting in stronger anticancer effect than ZnO (K1) sample Fig. 16. Reactive oxygen species

Fig. 10 XPS spectra of 3d for K2, K3, and K4 samples

(ROS), such as hydrogen peroxide (H_2O_2), superoxide anion (O_2^-), hydroxyl radicals ($\cdot\text{OH}$), and organic hydroperoxides (OHPs) are toxic to the cells as they damage cellular constituents such as DNA, lipids, and proteins and also lanthanum ions interact with thiol groups in proteins, ensuing in inactivation of respiratory enzymes and leading to the production of more reactive oxygen species (ROS) Fig. 17.

4 Conclusion

ZnO NPs (K1) and rare earth metal (REM) ions (La^{3+} , Ce^{3+} and Nd^{3+}) doped ZnO NPs were prepared through green method using *Gymnema sylvestre* leaves extract. Synthesized K1 (ZnO NPs), K2 (La doped ZnO NPs), K3 (Ce doped ZnO NPs) and K4 (Nd doped ZnO NPs) samples exhibit hexagonal wurtzite structure. Elemental oxidation state of Zn (2p), O (1s), La (3d), Ce (3d) and Nd (3d) were observed using XPS spectra. Morphological and elemental

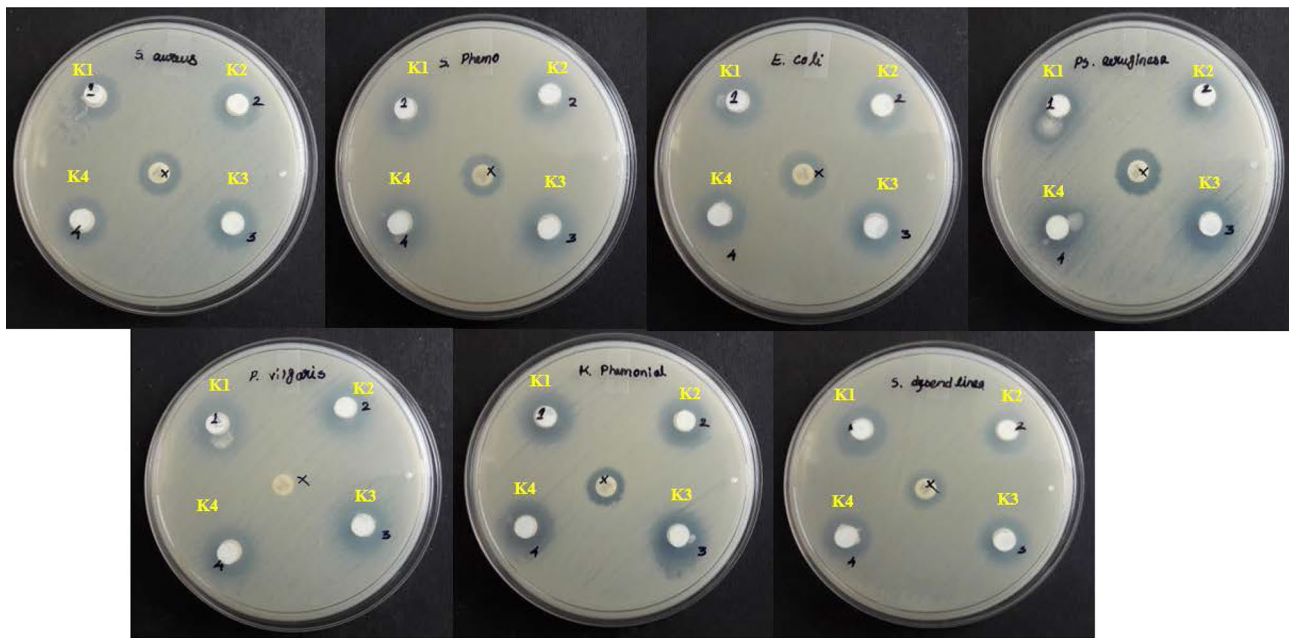


Fig. 11 The progress of antibacterial activity of K1, K2, K3 and K4 samples

Table 4 Comparative antibacterial values of present and various metals doped ZnO NPs on different bacterial strains

S.no	Concentration	Materials	Size (nm)	Bacteria
Present study				
1.	1.5 mg/ml	0.002% of La in ZnO	33	<i>Staphylococcus aureus</i> <i>Streptococcus pneumoniae</i> <i>Escherichia coli</i> <i>Klebsiella pneumoniae</i> <i>Pseudomonas aeruginosa</i>
2		0.002% of Ce in ZnO	27	
3		0.002% of Nd in ZnO	23	
Previous studies				
1	100 (µl)	0.03% of La in ZnO [39]	11.46	<i>Staphylococcus aureus</i>
2	1 (mg/ml)	0.01% of La in ZnO [40]	38	<i>Staphylococcus aureus</i> <i>Streptococcus pneumoniae</i>
3	10 (µg/ml)	0.03% of Ce in ZnO [41]	11.56	<i>Staphylococcus aureus</i>
4	1 (mg/ml)	0.05% Of Ce In ZnO [42]	32	<i>Staphylococcus aureus</i> <i>Streptococcus pneumoniae</i>
5	800 (µg/ml)	0.003% of Nd in ZnO [43]	33	<i>Escherichia coli</i> , <i>Klebsiella pneumoniae</i>
6	2 (mg/ml)	0.03% of Nd doped in ZnO [31]	35.2	<i>Pseudomonas aeruginosa</i>

composition were identified for the synthesized K1, K2, K3 and K4 samples using FESEM and EDAX spectra. Optical properties were estimated through UV-Vis and PL spectra. From the antibacterial activity, tested against clinical

pathogen using K1, K2, K3 and K4 samples. The K2 samples exhibits highest antibacterial effects as compared to other K1, K3 and K4 samples.

Fig. 12 The zone of inhibition formed around each disc, loaded with test samples indicated the antibacterial activity of **a** *S. aureus*, **b** *S. pneumoniae*, **c** *E. coli*, **d** *P. aeruginosa*, **e** *P. vulgaris*, **f** *K. pneumoniae* and **g** *S. synderiae* for the K1, K2, K3 and K4 samples

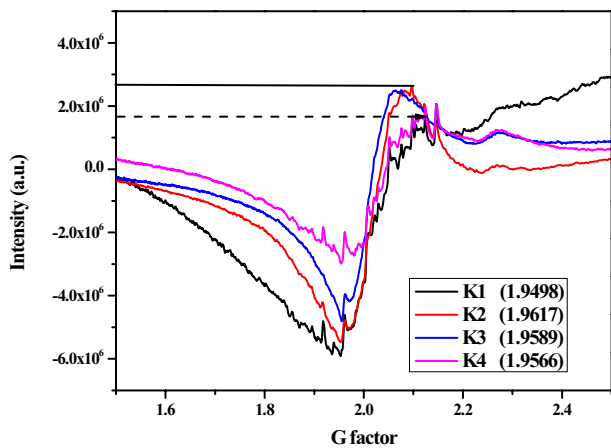
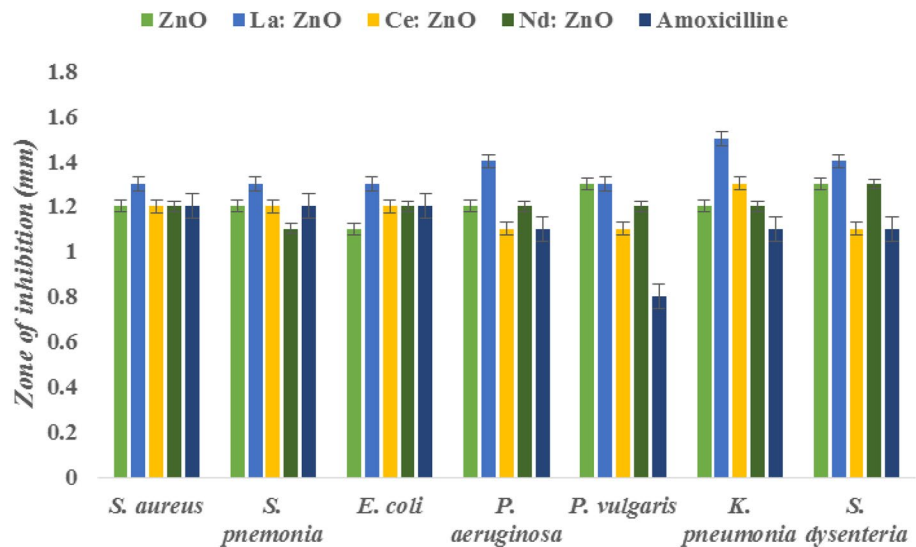


Fig. 13 EPR spectra of K1, K2, K3 and K4 samples

In vitro cytotoxicity effect were observed for A498 (human kidney carcinoma cell) and Vero (monkey kidney cell) lines. From practical therapeutic application, significant improvements are required to reduce the IC_{50} and to improve the cell specificity. The IC_{50} values obtained are (41.74, 35.86, 40.05 and 63.08 $\mu\text{g/ml}$) and (55.27, 49.69, 56.83 and 51.10 $\mu\text{g/ml}$) for K1, K2, K3 and K4 samples against A498 and Vero cells line. Minimum toxicity percentage was observed for synthesized all K1, K2, K3 and K4 samples using Vero cells. To traverse new strategies to develop the next generation of drugs or agents to control bacterial infections and cytotoxic effects the antibacterial and anticancer properties of ZnO and REM-doped ZnO NPs were examined.

Fig. 14 **a** Effect of K1, K2, K3 and K4 samples on the cytotoxicity property in human A498 cell (Kidney carcinoma cell). **b** Effect of K1, K2, K3 and K4 samples on the cytotoxicity property in Vero cell (African green monkey kidney cell)

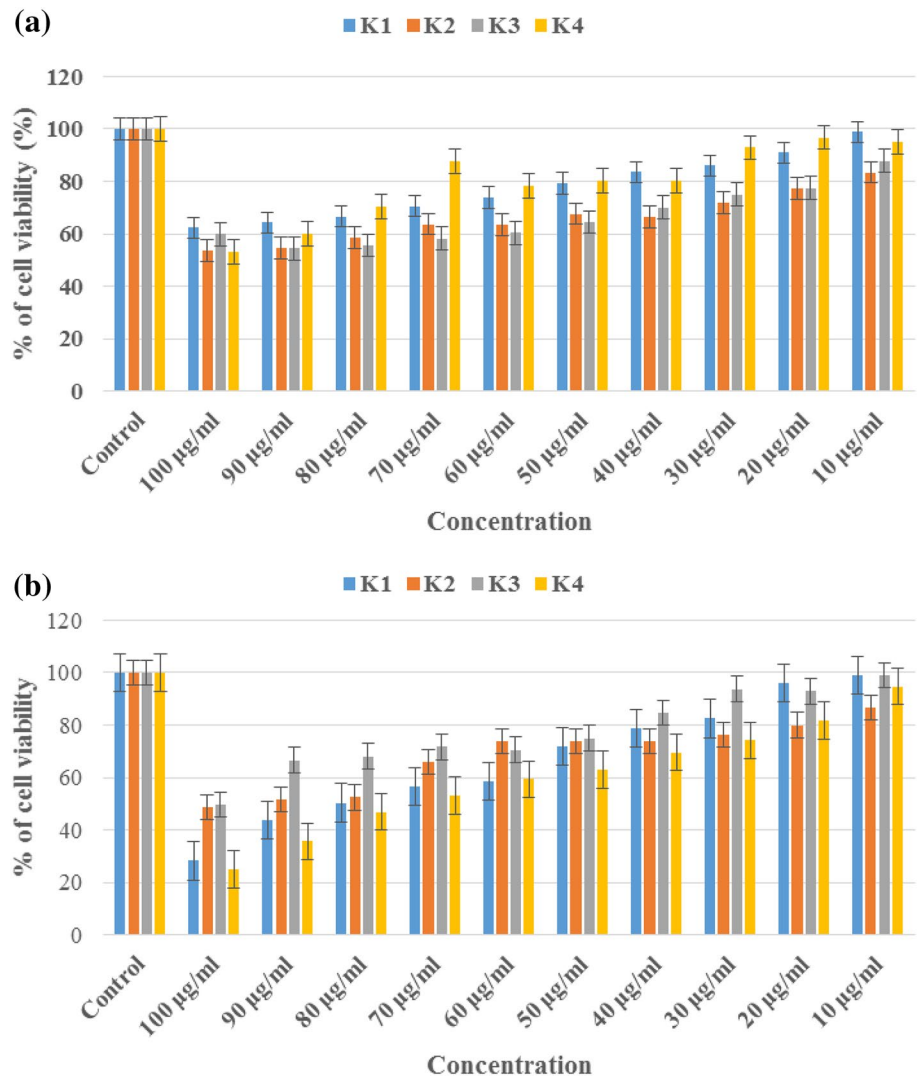
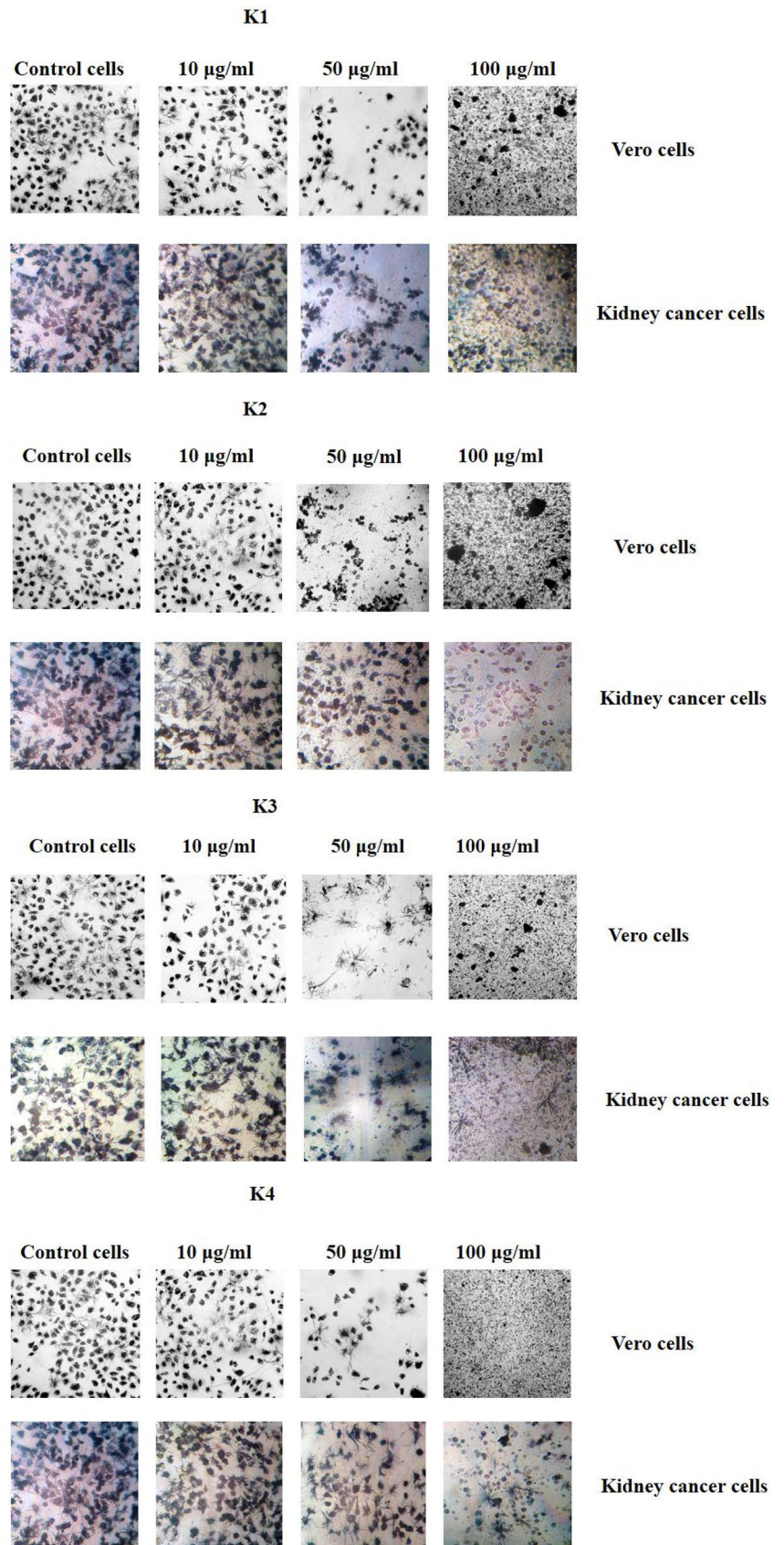


Table 5 Comparative IC₅₀ values of present and various metals doped ZnO NPs on cytotoxic response between the different cell types

Sample	IC ₅₀ concentration	Cell line		References
ZnO and La, Ce and Nd doped ZnO NPs (Present study)	41.74, 35.86, 40.05 and 63.08 µg/ml 55.27, 49.69, 56.83 and 51.10 µg/ml	Vero cells Kidney carcinoma cell		Present study
ZnO-2 and ZnO-4	41.85 µg/ml and 137.6 µg/ml	HeLa cell lines		[52]
ZnO	280 µg/ml	Human lung cancer cell line (A549)		[42]
Zn _{0.95} Ce _{0.05} O	82 µg/ml			
Zn _{0.90} Ce _{0.10} O	68 µg/ml			
Zn _{0.85} Ce _{0.15} O	76 µg/ml			
ZnO	121 µg/ml	MCF-7 Breast cancer cell line		[53]
ZnO	52.80 µg/ml	Human myeloblastic leukemia cell HL 60		[54]
ZnO	100 µg/ml	Human breast cancer MCF-7		[55]
ZnO	42.60 µg/ml	Human liver adenocarcinoma cell HepG2		[56]
Fe-doped ZnO	37.20 µg/ml			
Ag-doped ZnO	45.10 µg/ml			
Pd-doped ZnO	77.20 µg/ml			
Co-doped ZnO	56.50 µg/ml			
Doxorubicin	20.10 µg/ml			
ZnO	U87	HeLa	HEK	Human cerebral glioma tumor U87 [57]
ZnO micro-flower composed of nanorods	61.6 µg/ml	118 µg/ml	52.80 µg/ml	
	125 µg/ml	128 µg/ml	250 µg/ml	Cervical cancer HeLa
ZnO micro-flower composed of thin sheets	31.26 µg/ml	126 µg/ml	125 µg/ml	
ZnO microspheres composed of nanoparticles	30 µg/ml	61 µg/ml	62.5 µg/ml	Normal HEK cells
Silver Zinc oxide (Ag:ZnO)	20 µg/ml (MCF-7) 550 µg/ml (A549)			Human breast cancer (MCF-7) [58] Human lung cancer (A549)
Silver-zinc oxide nanocomposite (CD-Ag:ZnO NC)	50 µg/ml (MCF-7) 70 µg/ml (A549)			

Fig. 15 Kidney carcinoma cell (A498) and vero cells treated with K1, K2, K3 and K4 samples at the respective different concentration



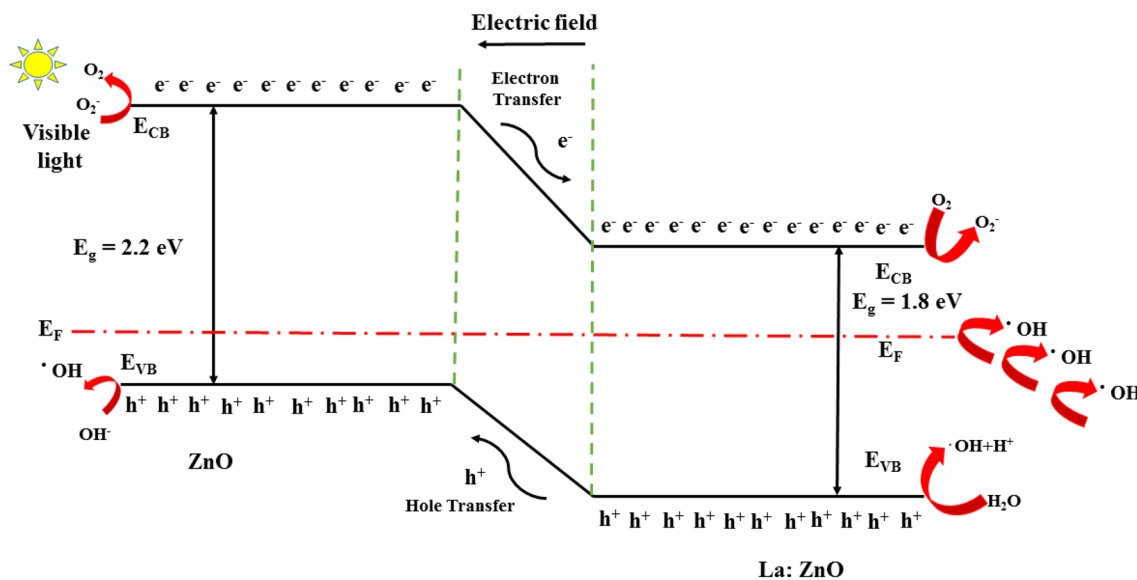


Fig. 16 The mechanism of the generation of reactive oxygen species from ZnO (K1) and La doped ZnO NPs (K2) induced by UV light

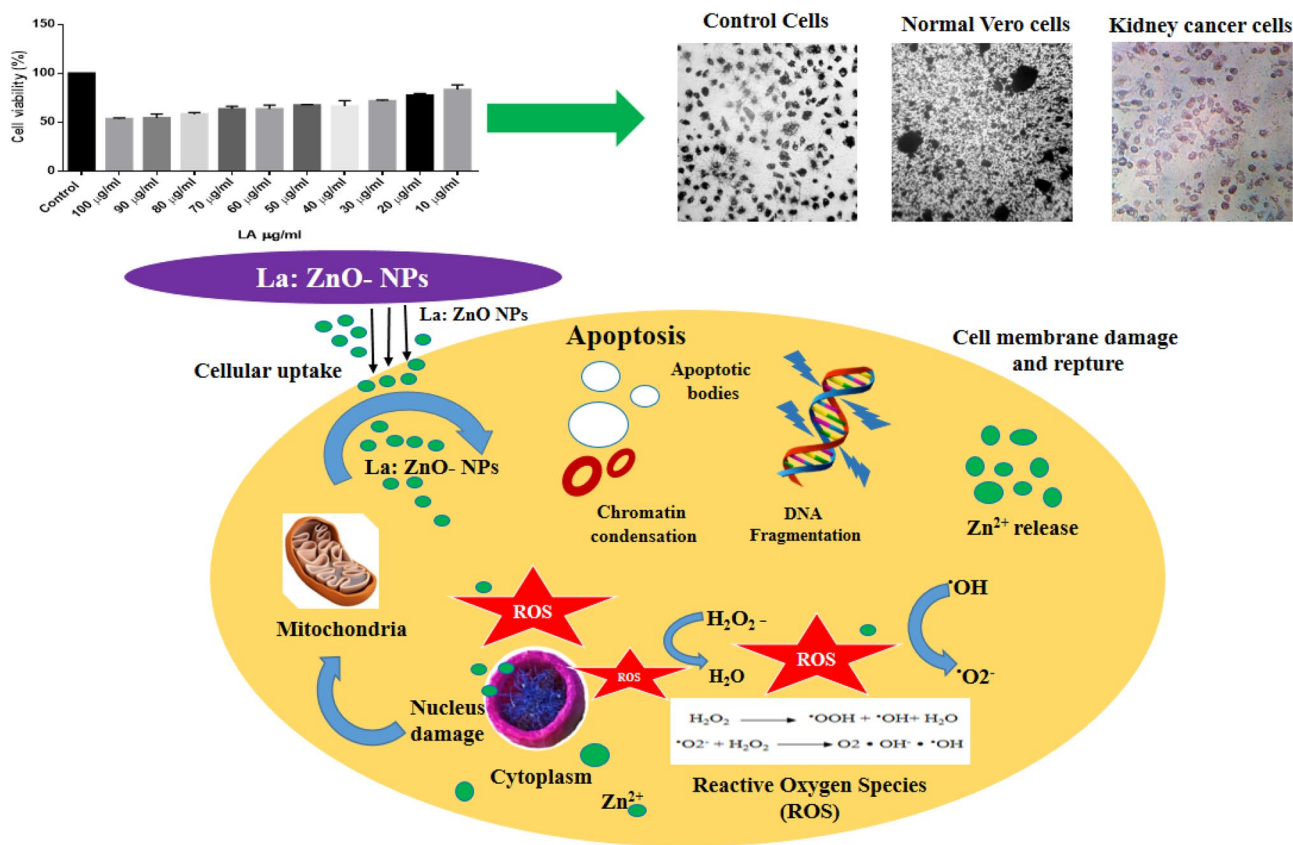


Fig. 17 Possible mechanisms underlying the cytotoxic activities leading to the cell death as caused by La doped ZnO NPs (K2)

Acknowledgements The authors are thankful to the members of Management committee and Principal of Jamal Mohamed College for providing necessary facilities.

Compliance with ethical standards

Conflict of interest The authors declare that they have no conflict of interest.

References

- Tang ZK, Wang GKL, Yu P (1998) Room-temperature ultraviolet laser emission from self-assembled ZnO microcrystalline. Thin films Appl Phys Lett 72(25):3270
- Zhou Z, Komori T, Ayukawa T, Yukawa H, Morinaga M, Koizumi A, Takeda Y (2005) Li- and Er-codoped ZnO with enhanced 1.54 μm photoemission. Appl Phys Lett 87(9):091109
- Wang X, Song J, Liu J, Wang ZL (2007) Direct-current nanogenerator driven by ultrasonic waves. Science 316(5821):102–105
- Armelaio L, Heigl F, Jurgensen A, Blyth RIR, Regier T, Zhou XT, Sham TK (2007) X-ray excited optical luminescence studies of ZnO and Eu-doped ZnO nanostructures. J Phys Chem C 111(28):10194–10200
- Song J, Wang X, Liu J, Liu H, Li Y, Wang ZL (2008) Piezoelectric potential output from ZnO nanowire functionalized with p-type oligomer. Nano Lett 8(1):203–207
- Vijayaprasath G, Ravi G, Haja Hameed AS, Mahalingam T (2014) Effect of cobalt doping on structural, optical, and magnetic properties of ZnO nanoparticles synthesized by coprecipitation method. J Phys Chem C 118(18):9715–9725
- Jeong WJ, Kim SK, Park GC (2006) Preparation and characteristic of ZnO thin film with high and low resistivity for an application of solar cell. Thin Solid Films 506:180–183
- Xu J, Pan Q, Shun YY, Tian Z (2000) Grain size control and gas sensing properties of tin oxide. Sens Actuators B 66:277–279
- Rekha K, Nirmala M, Nair MG, Anukaliani A (2010) Structural, optical, photocatalytic and antibacterial activity of zinc oxide and manganese doped zinc oxide nanoparticles. Phys B 405(15):3180–3185
- Dang Z, Fan L, Zhao S, Nan C (2003) Dielectric properties and morphologies of composites filled with whisker and nanosized zinc oxide. Mater Res Bull 38:499–507
- Yeber MC, Rodriguez J, Freer J, Duran N, Mansilla HD (2000) Photocatalytic degradation of cellulose bleaching effluent by supported TiO₂ and ZnO. Chemosphere 41(8):1193–1197
- Xu F, Zhang P, Navrotsky A, Yuan ZY, Ren TZ, Halasa M, Su BL (2007) Hierarchically assembled porous ZnO Nanoparticles: synthesis, surface energy, and photocatalytic activity. Chem Mater 19(23):5680–5686
- Jones N, Ray B, Ranjit KT, Manna AC (2008) Antibacterial activity of ZnO nanoparticle suspensions on a broad spectrum of microorganisms. FEMS Microbiol Lett 279(1):71–76
- Lang J, Han Q, Yang J, Li C, Li X, Yang L, Zhang Y, Gao M, Wang D, Cao J (2010) Fabrication and optical properties of Ce-doped ZnO nanorods. J Appl Phys 107(7):074302
- Singhal G, Bhavesh R, Kasariya K, Sharma AR, Singh RP (2011) Biosynthesis of silver nanoparticles using *Ocimum sanctum* (Tulsi) leaf extract and screening its antimicrobial activity. J Nanopart Res 13(7):2981–2988
- Sundrarajan M, Ambika S, Bharathi K (2015) Plant-extract mediated synthesis of ZnO nanoparticles using *Pongamia pinnata* and their activity against pathogenic bacteria. Adv Powder Technol 26(5):1294–1299
- Upadhyaya H, Shome S, Sarma R, Tewari S, Bhattacharya MK, Panda SK (2018) Green synthesis, characterization and antibacterial activity of ZnO nanoparticles. Am J Plant Sci 9(6):1279–1291
- Khan MF, Hameedullah M, Ansari AH, Ahmad E, Lohani MB, Khan RH, Alam MM, Khan W, Husain FM, Ahmad I (2014) Flower-shaped ZnO nanoparticles synthesized by a novel approach at near-room temperatures with antibacterial and antifungal properties. Int J Nanomed 9:853–864
- Zhang W, Bao S, Fang T (2016) The neglected nano-specific toxicity of ZnO nanoparticles in the yeast *Saccharomyces cerevisiae*. Sci Rep 6:24839
- Dheepakamalini T, Thiagasundaram T, Thanigavelan V, Kaliyamurthi V, Elansekaran S, Jegadeesan M (2012) Pharmacognostic and phytochemical studies on *Gymnema sylvestre* R. Br. Hairy Variant. Int J Pharm Phytopharmacol Res 2(3):143–147
- Vijayakumar P, Jafar Ahamed A (2017) Identification of bioactive compounds from the methanolic leaf extract of *Gymnema sylvestre*. J Adv Appl Sci Res 1:1–13
- Tiwari P, Mishra BN, Sangwan NS (2014) Phytochemical and pharmacological properties of *Gymnema sylvestre*: an important medicinal plant. Biomed Res Int 2014:19
- Jafar Ahamed A, Vijayakumar P (2017) Role of Zn and oxygen vacancies in green and chemically synthesised ZnO nanoparticles and their comparative in vitro toxicity studies for microbial and cancer cell (MCF-7) models. Int J Adv Sci Technol 5(3):67–73
- Møller P, Jacobsen NR, Folkmann JK, Danielsen PH, Mikkelsen L, Hemmingsen JG, Vesterdal LK, Forchhammer L, Wallin H, Loft S (2010) Role of oxidative damage in toxicity of particulates. Free Radic Res 44(1):1–46
- Li N, Sioutas C, Cho A, Schmitz D, Misra C, Sempf J, Wang M, Oberley T, Froines J, Nel A (2003) Ultrafine particulate pollutants induce oxidative stress and mitochondrial damage. Environ Health Perspect 111(4):455–460
- Desnues B, Cuny C, Gregori G, Dukan S, Aguilaniu H, Nystrom T (2003) Differential oxidative damage and expression of stress defence regulons in culturable and non-culturable *Escherichia coli* cells. EMBO Rep 4(4):400–404
- Aertsen A, Michiels CW (2004) Stress and how bacteria cope with death and survival. Crit Rev Microbiol 30(4):263–273
- Mosmann T (1983) Rapid colorimetric assay for cellular growth and survival: application to proliferation and cytotoxicity assays. J Immunol Methods 65(1–2):55–63
- Haja Hameed AS, Karthikeyan C, Senthil kumar V, Kumaresan S, Ravi G (2013) Impact of alkaline metal ions Mg²⁺, Ca²⁺, Sr²⁺ and Ba²⁺ on the structural, optical, thermal and antibacterial properties of ZnO nanoparticles prepared by co-precipitation method. J Mater Chem B 1:5950–5962
- Zandi S, Kameli P, Salamati H, Ahmadvand H, Hakimi M (2011) Microstructure and optical properties of ZnO nanoparticles prepared by a simple method. Phys B 406(17):3215–3218
- Vijayaprasath G, Murugan R, Palanisamy S, Prabhu NM, Mahalingam T, Hayakawa Y, Ravi G (2015) Structural, optical and antibacterial activity studies of neodymium doped ZnO nanoparticles. J Mater Sci Mater Electron 26(10):7564–7576
- Firdaus CM, Shah Rizamb MSB, Rusopa M, Hidayah SR (2012) Characterization of ZnO and ZnO: TiO₂ thin films prepared by sol-gel spray-spin coating technique. Procedia Eng 41:1367–1373
- Fan XM, Lian JS, Zhao L, Liu YH (2005) Single violet luminescence emitted from ZnO films obtained by oxidation of Zn film on quartz glass. Appl Surf Sci 252(2):420–424
- Mishra SK, Srivastava RK, Prakash SG, Yadav RS, Pandey AC (2010) Photoluminescence and photoconductive

- characteristics of hydrothermally synthesized ZnO nanoparticles. *Opto-Electron Rev* 18(4):467–473
35. Varghese N, Panchakarla LS, Hanapi M, Govindaraj A, Rao CNR (2007) Solvothermal synthesis of nanorods of ZnO, N-doped ZnO and CdO. *Mater Res Bull* 42(12):2117–2124
 36. Kumar N, Dorfman A, Hahm JI (2005) Fabrication of optically enhanced ZnO nanorods and microrods using novel biocatalysts. *J Nanosci Nanotechnol* 5:1915–1918
 37. Bagnall DM, Chen YF, Shen MY, Zhu Z, Goto T, Yao T (1998) Room temperature excitonic stimulated emission from zinc oxide epilayers grown by plasma-assisted MBE. *J Cryst Growth* 184(185):605–609
 38. Zhang Y, Zhou J, Si J (2017) Synergistic catalysis of nano-Pd and nano rare-earth oxide/AC: complex nanostructured catalysts fabricated by a photochemical route for selective hydrogenation of phenol. *RSC Adv* 7:54779–54788
 39. Manikandan A, Manikandan E, Meenatchi B, Vadivel S, Jagannathan SK, Lachumananandasivam R, Henini M, Maaza M, Aanand JS (2017) Rare earth element (REE) lanthanum doped zinc oxide (La: ZnO) nanomaterials: synthesis structural optical and antibacterial studies. *J Alloy Compd* 723:1155–1161
 40. Karthikeyan M, Jafar Ahamed A, Vijayakumar P, Karthikeyan C (2018) Green synthesis of pure ZnO and La doped ZnO nanoparticles and their structural, optical and antibacterial studies. *Eur J Biomed Pharm Res* 5(2):736–741
 41. Bomila R, Srinivasan S, Venkatesan A, Bharath B, Perinbam K (2017) Structural, optical and antibacterial activity studies of Ce-doped ZnO nanoparticles prepared by wet-chemical method. *Mater Res Innov* 22(7):379–386. <https://doi.org/10.1080/14328917.2017.1324379>
 42. Theivarasu C, Indumathi T (2017) Effect of Ce³⁺ metal ions on the antibacterial and anticancer activity of zinc oxide nanoparticles prepared by coprecipitation method. *Asian J Pharm Clin Res* 10(3):388–392
 43. Haja Hameed AS, Karthikeyan C, Ahamed AP, Thajuddin N, Alharbi NS, Alharbi SA, Ravi G (2016) *In vitro* antibacterial activity of ZnO and Nd doped ZnO nanoparticles against ESBL producing *Escherichia coli* and *Klebsiella pneumoniae*. *Sci Rep* 6:24312
 44. Tong GX, Du FF, Liang Y, Hu Q, Wu RN, Guan JG, Hu X (2013) Polymorphous ZnO complex architectures: selective synthesis, mechanism, surface area- and Zn-polar plane-codetermining antibacterial activity. *J Mater Chem B* 1:454–463
 45. Kappers LA, Gilliam OR, Evans SM, Halliburton LE, Giles NC (2008) EPR and optical study of oxygen and zinc vacancies in electron-irradiated ZnO. *Nucl Instrum Methods Phys Res B* 266:2953–2957
 46. Xu X, Xu C, Dai J, Hu J, Li F, Zhang S (2012) Size dependence of defect-induced room temperature ferromagnetism in undoped ZnO nanoparticles. *J Phys Chem C* 116(15):8813–8818
 47. Sivakumar P, Lee M, Kim YS, Shim MS (2018) Photo-triggered antibacterial and anticancer activities of zinc oxide nanoparticles. *J Phys Chem C* 30:1–47
 48. Sirelkhatim A, Mahmud S, Seeni A, Kaus NHM, Ann LC, Bakhori SKM, Hasan H, Mohamad D (2015) Review on zinc oxide nanoparticles: antibacterial activity and toxicity mechanism. *Nano-Micro Lett* 7(3):219–242
 49. Raghupathi KR, Koodali RT, Manna AC (2011) Size-dependent bacterial growth inhibition and mechanism of antibacterial activity of zinc oxide nanoparticles. *Langmuir* 27(7):4020–4028
 50. Bojarska M, Nowak B, Skowronski J, Piatkiewicz W, Gradon L (2017) Growth of ZnO nanowires on polypropylene membrane surface—characterization and reactivity. *Appl Surf Sci* 391:457–467
 51. Zhang H, Chen B, Jiang H, Wang C, Wang H, Wang X (2011) A strategy for ZnO nanorod mediated multi-mode cancer treatment. *Biomaterials* 32(7):1906–1914
 52. Krishna PG, Ananthaswamy PP, Mutta NB, Mariyappa KG, Singh R, Manchegowda SH, Dixit PS, Shivaprasad V (2017) Comparison of antimicrobial and anticancer activity of ZnO nanoparticles prepared using different precursors by hydrothermal synthesis. *J Chem Pharm Sci* 10(1):192–197
 53. Moghaddam AB, Moniri M, Azizi S, Rahim RA, Ariff AB, Navaderi M, Mohamad R (2017) Eco-friendly formulated zinc oxide nanoparticles: induction of cell cycle arrest and apoptosis in the MCF-7 cancer cell line. *Genes* 8(281):1–15
 54. Premanathan M, Karthikeyan K, Jeyasubramanian K, Manivannan G (2011) Selective toxicity of ZnO nanoparticles toward gram-positive bacteria and cancer cells by apoptosis through lipid peroxidation. *Nanomed Nanotechnol Biol Med* 7:184–192
 55. Chanu TI, Muthukumar T, Manoharan PT (2014) Fuel mediated solution combustion synthesis of ZnO supported gold clusters and nanoparticles and their catalytic activity and *in vitro* cytotoxicity. *Phys Chem Chem Phys* 16(43):23686–23698
 56. Ismail AFM, Ali MM, Ismail LFM (2014) Photodynamic therapy mediated antiproliferative activity of some metal-doped ZnO nanoparticles in human liver adenocarcinoma HepG2 cells under UV irradiation. *J Photochem Photobiol B Bio* 138:99–108
 57. Wahab R, Kaushik NK, Verma AK, Mishra A, Hwang IH, Yang YB, Shin HS, Kim YS (2011) Fabrication and growth mechanism of ZnO nanostructures and their cytotoxic effect on human brain tumor U87, cervical cancer HeLa, and normal HEK cells. *J Biol Inorg Chem* 16(3):431–442
 58. Sachdev A, Matai I, Gopinath P (2015) Dual-functional carbon dots–silver@zinc oxide nanocomposite: *in vitro* evaluation of cellular uptake and induction of apoptosis. *J Mater Chem B* 3(7):1217–1229
 59. Vijayalakshmi K, Sivaraj D (2016) Synergistic antibacterial activity of barium doped TiO₂ nanoclusters synthesized by microwave processing. *RSC Adv* 6(12):9663–9671

Publisher's Note Springer Nature remains neutral with regard to jurisdictional claims in published maps and institutional affiliations.